Published in final edited form as:
IEEE Trans Haptics. 2014 ; 7(2): 216–228. doi:10.1109/TOH.2013.36.

Validating a Population Model of Tactile Mechanotransduction of Slowly Adapting Type I Afferents at Levels of Skin Mechanics, Single-unit Response and Psychophysics

Gregory J. Gerling [Member, IEEE], **Isabelle I. Rivest**, **Daine R. Lesniak [Student Member, IEEE]**, **Jacob R. Scanlon**, and **Lingtian Wan**
Department of Systems and Information Engineering, University of Virginia, Charlottesville, VA 22904

Abstract

Previous models of touch have linked skin mechanics to neural firing rate, neural dynamics to action potential elicitation, and mechanoreceptor populations to psychophysical discrimination. However, no one model spans all levels. The objective of work herein is to build a multi-level, computational model of tactile neurons embedded in cutaneous skin, and then validate its predictions of skin surface deflection, single-afferent firing to indenter shift, and population response for sphere discrimination. The model includes a 3D finite element representation of the distal phalange with hyper- and visco-elastic mechanics. Distributed over its surface, a population of receptor models is comprised of bi-phasic functions to represent Merkel cells' transformation of stress/strain to membrane current and a leaky integrate-and-fire neuronal models to generate the timing of action potentials. After including neuronal noise, the predictions of two population encoding strategies (Gradient Sum and Euclidean Distance) are compared to psychophysical discrimination of spheres. Results indicate that predicted skin surface deflection matches Srinivasan's observations for 50 micron and 3.17 mm diameter cylinders and single-afferent responses achieve R^2=0.81 when compared to Johnson's recordings. Discrimination results correlate with Goodwin's experiments, whereby 287 and 365 m^{-1} spheres are more discriminable than 287 and 296 m^{-1}.

Keywords

Tactile; sensation; skin mechanics; SAI; mechanoreceptor; finite element model; leaky integrate-and-fire; neural dynamics; biomechanics; psychophysics

1 Introduction

Our sense of touch is essential for performing everyday tasks such as eating and dressing. To those living with upper limb loss, performing such tasks can present serious challenges. To enable the next generation of tactile and proprioceptive prosthetics, in addition to furthering

E-mail address of corresponding author: gg7h@virginia.edu.

our scientific understanding, a significant body of work has sought to understand how biological receptors work, alone and in populations.

Tactile sensation is typically studied at either of two levels: electrophysiological recordings or psychophysical responses [1]. Single-afferent, electrophysiological recordings are performed by connecting a microelectrode to an afferent fiber and timing the spikes as the end organ in the skin is stimulated mechanically [2]. Psychophysical experiments, on the other hand, relate distal stimuli to human behavioral response [3] by measuring absolute thresholds and difference discrimination. Psychophysical experiments assume that perception is based upon information from a population of receptors, something presently unobservable due the difficulty in simultaneously recording from hundreds of afferents. Therefore, these two experimental approaches have been augmented by the use of models, at various levels of detail.

At the level of the skin, elasticity models have sought to link mechanics to the neural response elicited by the indentation of rigid stimuli. Continuum mechanics [4], [5] and finite element [6] techniques can calculate distributions of stress and/or strain, which are converted into firing rates via scaling functions. While skin models enable the prediction of firing rates, most do not predict the timing of individual action potentials.

At the level of single afferents, neural dynamics models have sought to approximate the elicitation of individual action potentials. In addition to two-dimensional reductions of the classic Hodgkin-Huxley equations, leaky integrate-and-fire (LIF) models [7], [8] have been specialized to produce spike times when membrane potential is driven to threshold, typically as a function of vibration frequency and magnitude. Predicting the timing of individual spikes, as opposed to gross firing rate, is important for matching behaviorally relevant neural codes, such as first spike latency [9]. Although tied together *in vivo*, neural dynamics and skin mechanics models have largely been used in isolation.

In contrast to the physics-based models, data-driven approaches tie stimulus characteristics to empirically observed neural firing behaviors, usually via regression and fitted functions. For example, Johnson identified that rapidly adapting (RA) afferents exhibit a piecewise relationship between firing rate and peak amplitude of vibration [10]. Similarly, Wheat and Goodwin used regression to tie firing rate for slowly adapting type I (SAI) afferents to the curvature of annular stimuli and the distance between the stimulus and receptive field center [11]. Significant work by Johansson, et al. has used the recruitment sequence of a population of afferents to predict the direction and orientation of indentation, given just the timing of first spikes [9], [12] or just the afferents near the fingernail [13]. The drawback is that data-driven approaches abstract underlying physiological and neural mechanisms, and their input-output relations are linked tightly to the stimulus utilized.

No one effort has sought to align model predictions at multiple levels, linking skin mechanics to firing rates, neural dynamics to single spike elicitation, and mechanoreceptor populations to psychophysical discrimination. Therefore, the work herein seeks to bridge a gap between empirical models which abstract the physics of the skin and receptor and physics-based models that either link skin mechanics to firing rate but cannot generate spike

timing, or link receptor dynamics to spike timing but leave out the attenuation of the skin. Perhaps most significantly, this work explores means to predict a psychophysical response, using two population encoding approaches. Because of its prominent role in spatial perception [14], studied herein, the SAI afferent of the glabrous skin is the focus of this work.

2 Overview of Methodology

Herein, a computational model of the cutaneous skin and tactile neuron is assembled, its free parameters fit, and its input-output relationships validated against existing data at three levels. The model combines a 3D finite element representation of the fingertip to mimic skin mechanics, a bi-phasic transduction function to convert stresses and strains in the simulated skin into transmembrane current at the SAI receptive end-organ, and a leaky-integrate-and-fire model to generate the timing of spikes. To form a population that responds over the fingertip's surface, the base model is duplicated by the number of desired afferents. Then two population encoding strategies are utilized, Euclidean Distance and Gradient Sum, to predict the psychophysical response. Model fitting identifies values for six free parameters to best mimic recorded SAI firing rates. Model validation compares: a) predicted skin surface deflection to that observed for a human fingertip when indented with cylinders of different curvature, b) predicted firing rates for single receptors to those recorded from SAIs in the primate fingertip in response to a 3.0 mm block indented at 0.2 mm increments, and c) predicted population responses to discrimination thresholds obtained in human psychophysical experiments for a set of spheres.

2.1 Computational Model

The subparts of the computational model represent skin elasticity mechanics, receptor membrane transduction at the site of the SAI end organ, and neural dynamics. This single-unit receptor model is then extended to create a population of SAI afferents with a density of 100 mm^2.

2.1.1 Skin mechanics sub-model—A 3D finite element model (FEM) of the human distal phalange simulates the propagation of stress and strain through skin layers upon deformation of the finger surface. The FEM approximates the thickness and material properties of the skin's microstructures, including the epidermis, dermis, subcutaneous tissue, and distal phalange (Figure 1). Skin thickness was informed by human tissue measurements [15], [16], and hyper- and visco-elastic material properties through previous testing [17], [18]. The anisotropic nature of the skin was not included. Material property selection is discussed in depth in Section 2.2.1.

A mesh of approximately 232,000 nodes and 276,000 elements was created using TrueGrid (XYZ Scientific Applications Inc., Livermore, CA), and Patran (MSC Software, Santa Ana, CA) software. The mesh uses 8-node linear brick hybrid with constant pressure elements (C3D8H) with 0.1 mm edge lengths at the epidermal-dermal border and exterior surface.

This edge length affords a volume that approximates that of the end-organ for a SAI, the Merkel cell-neurite cluster. It also allows for smoother deflection of the skin surface in

response to highly curved stimuli as compared to other models built by the authors previously [19]. The inner dermis, subcutaneous tissue and bone geometry employ reduced mesh resolution as they are further from the exterior surface and receptor sites. The larger and fewer internal elements vastly improve runtime during analysis. The interior of the mesh utilized 6-node wedge elements (C3D6H) in combination with larger 8-node brick elements. Nodes along the nail and bone were constrained in x, y, and z dimensions to replicate experiments in which the nail is glued to a surface [20], [2].

To inform neural predictions, strain energy density (SED) is sampled at the epidermal-dermal border, 0.471 mm from the skin surface [21] and serves as input into the transduction sub-model. SED is one possible measure of stress and strain extracted by the SAI end organ [6], [22], [17], [18], [23], though it may alternatively respond to maximum compressive stress, maximum compressive strain, von Mises stress, or another quantity [5], [24], [25]. While the exact measure is unresolved and quite difficult to decipher, SED well correlates to static firing rate. All finite element analysis was performed using ABAQUS Standard, version 6.6.

2.1.2 Receptor membrane transduction sub-model—SED sampled at a given element in the FEM is transformed into current, which parallels how SED in the vicinity of the Merkel cells is transformed into current across the SAI membrane. While sigmoidal functions have been used to transform SED into current [26], this work employs two linear functions to differentially respond to the dynamic ramp (i.e., high spike firing during stimulus movement) and static hold phases (i.e., slower firing during sustained indentation) with fewer model parameters. The transduction function (Eqn. 1 and 2 converts SED, $U_o(t)$ Pa, and change in SED, $U_o'(t)$ Pa/ms, into current, $I(t)$ mA, using three coefficient terms: an intercept constant, β mA, a dynamic gain, k_d mA · s/Pa, and a static gain, k_s mA/Pa. Variable h in Equation 2 represents the 0.001 ms time increment used in calculating change in SED over time. The dynamic term, $k_d \cdot U_o'(t)$, responds to first-order change in SED, and thus dominates during the early period when the indenter is moving, while the static term contributes mainly thereafter.

$$I(t) = \beta + K_d \cdot U_o'(t) + K_s \cdot U_o(t) \quad (1)$$

$$U_o' = \left\{ \begin{array}{ll} 0, & t = onset \\ \left| \frac{U_o(t) - U_o(t-h)}{h} \right|, & t \neq onset \end{array} \right\} \quad (2)$$

Parameters β, k_d, and k_s were determined through model fitting (Section 2.2.2).

2.1.3 Neural dynamics sub-model—A leaky-integrate-and-fire model of neural dynamics transforms membrane current into spike times. The SAI membrane is abstracted as a resistive-capacitive circuit (Eqn. 3) with time constant τ ms. As current, $I(t)$ mA, passes through the SAI membrane (with resistance R ohms and capacitance C mF), membrane potential, $u(t)$ mV, accumulates (Eqn. 4). Once this potential reaches a predetermined threshold, $\overline{v}$ mV, the time is noted as a spike time, membrane potential is reset to resting

potential, and a 1.0 ms refractory period is entered [27]. When the refractory period terminates, the process repeats until the stimulus is removed.

$$\tau = RC \quad (3)$$

$$I(t) = \frac{u(t)}{R} + C \cdot \frac{\partial u}{\partial t} \quad (4)$$

Equations 3 and 4 can be rewritten as a single differential equation which defines change in membrane potential as a function of membrane potential, current, and time. Equation 5 is solved using a fourth-order Runge-Kutta numerical method to determine membrane potential one timestep in the future, $U_{t_{i+1}}$. Initial membrane potential, U_{t_0}, is set to 0.

$$g(u,t) = \frac{\partial u}{\partial t} = \frac{-u(t)}{\tau} + \frac{I(t)}{C} \quad (5)$$

Parameters τ, C, and $\bar{v}$ are determined through model fitting (Section 2.2.2).

2.1.4 Model extension to populations of receptors—To form the response of a population of receptors, we sample SED at multiple locations at the epidermal-dermal border of the FEM (0.471 mm depth). Individual SED samples are then input to transduction and neural dynamics sub-models, as described above. With this setup, the model is configured into a population density of 100 receptors per cm^2, which seeks to match that observed for SAI populations of the human fingertip [28]. The population layouts used in this work are rectangular, though random and Gaussian layouts have been investigated by the authors previously [29]. More detail on the two population encoding strategies is provided in Section 2.2.3.

2.2 Numerical Experiments for Model Validation

Model validation is performed by comparing model output to observed data at three points: skin mechanics, single-unit response, and population response (Figure 2).

2.2.1 Skin mechanics validation—The test of skin surface deflection provides insight into the bulk mechanical response of the combined tissue layers. The displacement at the surface of the skin (dependent variable) is measured in response to 50 micron line load and 3.17 mm cylinder indenters displaced 1.0 mm perpendicular to the long axis of the finger (independent variables). Predicted skin surface deflection is compared to Srinivasan's observations, taken approximately every 0.05 mm of the imaged skin surface in response to actual indentation [30], [31]. Nodal displacement measurements along the center line of the fingertip surface are taken at the final deformation depth near the indentation site.

To determine the material properties of modeled tissue layers that best approximate the observed behavior, three trials were conducted. Trial 1 models all skin layers as linear elastic [18] and used a viscoelastic Prony series with parameters listed in Table 1 [17]. Trial 2 uses linear elastic properties (Table 2) for the epidermis and bone, but models the dermis

and subcutaneous fat as hyperelastic using a polynomial N=2 model [17]. Trial 3 combines the softer epidermis and bone from Trial 1 and the hyper-elastic dermis and subcutaneous tissue from Trial 2.

2.2.2 Single-unit fitting using cross-validation—Single-unit predictions are fit to published SAI electrophysiological firing rates [2] using a cross-validation framework. Within this framework model parameters β, k_d, k_s, τ, C, and $\bar{v}$ are fit using response surface methodology (RSM) [32].

In brief review of Phillips and Johnson's experimental procedure, *in vivo* electrophysiological recordings were performed with primate SAI afferents [4]. The procedure sought to determine rates of spike elicitation as a 3.0 mm bar was indented in the finger pad to a depth 1.0 mm. The bar was then laterally shifted in discrete 0.2 mm intervals across the SAI's receptive field to determine the firing rate (dependent variable) as the distance between indenter and the center of the SAI receptive field increased (independent variable). For each indentation, spikes were recorded for 1.0 s and converted to firing rates. Each indentation was a ramp-and-hold stimulus, where the ramp-up occurred from 0 to 50 ms and the hold occurred from 51 to 1,000 ms. An example of the idealized recordings, which exhibits features typical of SAI afferents, is displayed in Results (Figure 5).

As in Phillips and Johnson's mechanical stimulation procedure, the independent variable is the lateral location of the 3.0 mm bar relative to the receptive field center, and the base dependent variable is spike times. Two derived dependent variables, firing rate during the dynamic ramp-up and static hold phases, are calculated from spikes elicited in either phase. These time windows are 30 – 50 ms and 600 – 950 ms, respectively. The dynamic window was set because it includes the highest frequency firing, and the static window was chosen to match the recording window set by Phillips and Johnson. Firing rates for the dynamic ramp and static hold phases are calculated by averaging the reciprocal interspike intervals (*ISI*) for spikes in the respective time window (Equations 6, 7, 8, 9, 10), where *m*-*l*= number of ISIs in dynamic window, *p*-*n* =number of ISIs in static window, f_d=firing rate in the dynamic ramp phase, f_s=firing rate in the static hold phase.

$$ISI_i = t_i - t_{i-1} \quad (6)$$

$$ISI_d = \frac{1}{m-l} \Sigma_{i=l}^{m} ISI_i \quad (7)$$

$$ISI_s = \frac{1}{p-n} \Sigma_{i=n}^{p} ISI_i \quad 8$$

$$f_d = \frac{1}{ISI_d} \quad (9)$$

$$f_s = \frac{1}{ISI_s} \quad (10)$$

A third derived dependent variable is the modulation index, which compares the firing rate when the edge of the stimulus (R_{max}) compared to the flat part of the stimulus (R_{min}) is directly above the receptive field center.

$$modulation\_index = \frac{R_{max} - R_{min}}{R_{max} + R_{min}} \quad (11)$$

Employing a cross-validation framework to estimate the out-of-sample performance of the model, 36 indenter shift locations are partitioned into six subsets of equal size prior to fitting. Table 3 shows training and testing partitions for the six folds. For each subset j, the model is fit using the shift locations in the five subsets excluding j (training set), and then evaluated against subset j (testing set). The estimate of out-of-sample performance is obtained by averaging the performance measure for each j. Evaluating the model in this way allows each data point to efficiently contribute to estimates of both model parameters and performance while mitigating the risk of model over-fitting associated with in-sample performance estimates.

The six free model parameters, β, k_d, k_s, τ, C, and $\bar{v}$ are fit within the cross validation framework using response surface methodology. The goal is to find a combination of values which maximize a weighted goodness of fit measure, fractional sum of squares (FSS), between model predictions and the *in vivo* firing rates for like stimuli. In Equations 12, 13, and 14, a total FSS is calculated by adding weighted contributions from static hold (weighing factor ω_s) and dynamic ramp (weighing factor ω_d) phases. The weight of the static hold is set to three times greater than dynamic ramp because its duration is greater. The variable $(obs\_f_d)_i$ refers to the *in vivo* firing rate for the dynamic ramp phase for location-grating shift i, and $(pred\_f_d)_i$ corresponds to dynamic phase model predictions for shift i. Likewise, $(obs\_f_s)_i$ and $(pred\_f_s)_i$ refer to *in vivo* and predicted firing rates for the static hold phase.

$$FSS = \omega_d \cdot FSS_d + \omega_s \cdot FSS_s \quad (12)$$

$$FSS_d = 1 - \frac{\Sigma_{i=1}^{30}[(obs\_f_d)_i - (pred\_f_d)_i]^2}{\Sigma_{i=1}^{30}(obs\_f_d)_i^2} \quad (13)$$

$$FSS_s = 1 - \frac{\Sigma_{i=1}^{30}[(obs\_f_s)_i - (pred\_f_s)_i]^2}{\Sigma_{i=1}^{30}(obs\_f_s)_i^2} \quad (14)$$

Within each fold, RSM fitting is performed twice, with two sets of starting parameters. Multiple sets of starting parameter values help guard against finding a local optimum when following the path of steepest ascent. The set of parameters for the first start point is $\beta = 0$

mA, k_d = 8e-09 mA · Pa/ms, k_s = 7e-07 mA/Pa, τ = 68 ms, C = 1e-06 mF, and $\bar{v}$ = 50 mV. The set of parameters for the second start point involved changes only to k_d (8.2e-09 mA · Pa/ms) and k_s (3.0e-07 mA/Pa).

The iterative RSM procedure follows 5 steps. First, base model parameters β, k_d, k_s, τ, C, and $\bar{v}$ are set and a coding increment (Δk) is chosen for each parameter through trial and error. Increments are chosen such that they caused small deviations in model output, and are typically two orders of magnitude smaller than the base parameters. Once the base parameters and coding increments are set, the base parameters are systematically incremented and decremented by one coding increment and *FSS* is calculated for each of the 2^6 combination of parameters as well as the unmodified base parameters, for a total of 65 runs. A linear regression approximates the relationship between model parameters and *FSS.* The regression coefficients are then used to determine the magnitudes and direction in which to vary all six model parameters to obtain a larger value of *FSS.* The model is run using parameters found by taking successive steps following this path of steepest ascent until no further gains are achieved. At this point, the process is repeated using the parameters obtained by following the path of steepest ascent. The procedure iterates until *FSS* between observed and predicted firing rates no longer increases.

2.2.3 Population validation at psychophysical level—A psychophysical task of sphere discrimination is used to validate the prediction of the population of receptors. In specific, we investigate the ability of the model, configured in a population density of 100 receptors per cm^2, to discriminate indenters with radii of curvature (RC) between 296 and 365 m^{-1} from a standard indenter with RC 287 m^{-1}. This procedure aligns with Goodwin's previous work to characterize human discrimination [20], which indicated that participants could distinguish a curvature of 365 m^{-1} from a standard of 287 m^{-1} in 95% of trials and an RC of 296 m^{-1} from the standard in 58% of trials, i.e., a value slightly above chance performance.

As in Goodwin's procedure, the FEM is indented with spherical indenters with RCs from 287 to 365 m^{-1} to a depth of 1.0 mm with a ramp-up period of 50 ms and a hold period of 950 ms. The psychophysical prediction is made by following the steps in Figure 3. First, (a) noise is introduced by multiplying firing rates and first spike latencies of all elements in one indentation, e.g. RC 287 m^{-1}, by a set of normal random variables with mean μ1=1 and standard deviation σ1. The value for σ1 was varied between 0.015 and 0.085. Then, either the Gradient Sum or Euclidean Distance method was employed to link modeled population responses to the discrimination task. Two methods were used as the exact nature of the biological process is unclear (see *Discussion*).

Gradient Sum Method: With this approach, basically, each indenter is represented by a single number, which can be compared to other spheres. The method traverses the population receptor by receptor and calculates, for each, a gradient from its neighbors' firing rates or first spike latencies. In specific, in step (b), an element-to-neighbors gradient is calculated by summing absolute values of differences between the element and its neighboring elements; (c) gradient sum is then obtained by summing gradients of all elements in a population. In (d), 100 gradient sums are obtained for one sphere by repeating

(a), (b) and (c) 100 times, each time with a new set of normal random variables with the same mean value and standard deviation. In (e), by repeating (a), (b), (c) and (d) for all 7 RCs, 700 gradient sums, 100 per RC, are generated and μ2, σ2 are calculated for each RC. The process hereto is repeated in (f) to obtain 100 μ2, σ2 values per indenter. A signal detection theory approach was used to compare the standard, RC 287, with the other spheres. For example, in (g, h) one set of μ2, σ2 predictions for RC 287 m^{-1} and one from RC 296 m^{-1} are randomly picked as inputs for the signal detection theory method. A β criterion of 0.5 was used as default in the signal detection theory method outputting 1 hit rate (HR 1) for the indentation of RC 296 m^{-1}; (i) by repeating (g), (h) 100 times, 100 hit rates are generated for RC 296 m^{-1}; (j) by repeating (g), (h), (i) for all RCs, 600 hit rates are obtained, 100 for each sphere, excluding the standard, RC 287 m^{-1}; (k) psychophysical predictions are generated using hit rates obtained, and the mean μ3 and standard deviation σ3 error bar of those hit rates are obtained.

A derivative of the Gradient Sum method (not shown in its entirety in Figure 3) was also used whereby the β criterion was varied as a normal random variable. In this case, all procedures (a-d) remained the same except at step (e) 5000 sums per RC were generated instead of 100. Steps (f and g) were skipped. At (i and j), we generated 100 hit rates per indenter based on shifts of beta as a normal random variable (1, 0.01) and (1, 0.02). That is, we completed 100 hit rates of different betas for a fixed mean, standard deviation for 287 m^{-1} compared to that for 296 m^{-1}. By changing from 0.01 to 0.02 we were able to increase the error bars, while keeping the mean probability of detection unchanged.

Euclidean Distance Method: With this approach, basically, firing rates and first spike latencies can be compared, receptor by receptor, for populations indented with different spheres. Therefore, the capability to discriminate is based upon the difference in predicted firing rates, or first spike latencies, compared receptor by receptor between the indentations of two spheres, and then summed. In specific, in step (b*), all 18 noisy firing rates and first spike latencies form a set, e.g. set 1, where the 18 noisy firing rates represent the 18 elements in a population of 100 receptors/cm^2; (c*) 100 sets are obtained for each sphere by repeating (a) and (b*) 100 times, each time with a new set of normal random variables with the same mean value and standard deviation. In (d*), 700 sets, 100 for each RC, are generated by repeating (a), (b*) and (c*) for all 7 RCs. In (e*), one set from RC 287 m^{-1} and one from another indenter, e.g. RC 296 m^{-1}, are randomly selected, and by subtracting corresponding values element by element and summing the 18 absolute values of differences, 1 sum is obtained; (f*) by repeating (e*) 100 times, 100 sums for each RC are generated; (g*) by repeating (e*), (f*) for all 7 RCs, 700 sums, 100 for each RC, are generated. A decision rule (h*) was used to classify a sum as a hit or miss, where sums per RC (296 to 365 m^{-1}) were compared against the midpoint of the prediction of that RC's mean and that of the standard. This decision rule was repeated 100 times per indenter to generate 100 hit rates, with μ3, σ3 used to attain psychophysical predictions.

Note that in all cases where the β criterion was fixed, we were able to control the mean probability of detection by changing the normal random variable in Figure 3, step (a). When we change, in step (a), the 100 generated matrices to 10 we increase the standard deviation on the probability of detection. Similarly, when we calculate 10 hit rates, instead of 100, the

mean probability of detection is not stable, i.e., if 10 hit rates are generated and then 10 hit rates again, the predictions change.

In this way, psychophysical predictions for spheres indented in two shift positions (0.0 and 0.2 mm along proximal-distal axis) ensure that performance is consistent regardless of a slight variation in the indentation.

3 Results

3.1 Skin Mechanics Validation

Material properties for the FEM were varied and the resulting models were indented with cylinders of radii 50 microns and 3.17 mm. Figure 4 shows the skin surface deflection results. Two regions of the plot can be inspected: that closest to the site of indentation (approximately 0.5 mm and closer) and that further away (0.5 to 5 mm). In the case of the 50 μm indenter, material properties for Trial 1 produce deflection results that overshoot observed data in both regions and material properties in Trial 2 produce results that undershoot observed data. Trial 3, which used a combination of material properties from the first two trials, produced surface deflection similar to the observed data in both regions.

3.2 Single-unit Fitting using Cross-Validation

Table 4 provides intermediate and final values for the six model parameters and in-sample *FSS* for each set of parameters in one RSM session (fold 3, start point 2). In this session, six iterations of RSM were completed before *FSS* no longer increased and *FSS* rose from 0.77 to 0.82. Final model parameters are in bold at the bottom of the table.

Predicted firing rates during the dynamic ramp and static hold phases overlay observed firing rates for a 3.0 mm bar (Figure 5). Modulation indices are shown in Table 5. In the dynamic ramp phase, minimum and maximum firing rates average 54 and 212 spikes/s, respectively. Given the calculation for modulation index in Equation 11, the proximity to an edge increased firing rate by up to 157 spikes/s. The edge effect is less drastic for the static hold phase, with a modulation index of 52 spikes/s.

3.3 Population Validation at Psychophysical Level

Figure 6 shows example 3D plots of firing rate response produced for dynamic ramp and static hold phases of the indentation, as well as first spike latency.

Figures 7 and 8 show the results of the probabilistic population encoding compared to Goodwin's psychophysical results. In Figure 7, plots (a)-(c) show the results for firing rate and first spike latency prediction using the Gradient Sum method. The predicted firing rate in the static hold led to the best fit to the experimental data and was robust to the 0.2 mm lateral shift. In contrast, while both firing rate in the dynamic hold and first spike latency increase monotonically, the two predictions (dotted lines in each plot) diverge given the 0.2 mm lateral offset. Figure 7, plot (d) shows the results in the static hold phase using the Euclidian Distance method.

Figure 7, plots (e, f) can be compared to plot (a) and indicate that the means can be increased or decreased by reducing or increasing afferent to afferent noise, respectively, per parameter σ1. Figure 7, plot (g) indicates that the error bars on the psychophysical predictions can be increased by changing the procedure (a) in Figure 3, whereby only 10 normal random noise matrices are used instead of 100. Another means of controlling the error bars is via the β criterion in the signal detection theory step, Figure 8. In this case, we varied the β criterion by a small amount from trial to trial by drawing from a distribution with a tighter variance (0.01, Figure 8 (a)) and were able to achieve a greater or lesser change to the error bars, for example, as compared to when the variance was modified to 0.02 in Figure 8 (b).

4 Discussion

This work develops and validates a multi-level, physics-based model for the SAI afferent that combines skin mechanics and neural dynamics to enable a psychophysical prediction of a range of spatial stimuli. The model's validation is done at three levels and indicates, in particular, that 1) the FE model's surface deflection closely matches that observed in Srinivasan's human experiments [30], 2) the single-unit results achieve an *FSS* of 0.81 which compares favorably to Johnson's neural recordings and modeling efforts [4] [26] while incorporating an ability to respond to the rate of indentation, and 3) the results of the simulated psychophysical sphere discrimination correlate with Goodwin's experiment [20] and indicate the model can differentiate between spheres of RC 287 and 365 m^{-1}, two indenters that are distinguishable with $p \approx 1$.

Perhaps most significantly, the work explores means to predict a psychophysical response using two approaches, Euclidean Distance and Gradient Sum. Two significant extensions with this type of multi-unit, physics based model are that different single unit metrics can be tied to population coding, and other sources of information could be accounted, such as rapidly adapting afferents and only those afferents near the edge of the nail.

4.1 Simulating a Psychophysical Response

We introduced two strategies for simulating a population of afferents and making probabilistic psychophysical prediction. With the Euclidean Distance method, the capability to discriminate two indenters is based upon the difference in predicted static firing rates, compared receptor by receptor and then summed, between the standard and comparison stimuli. In contrast, the Gradient Sum method traverses receptor by receptor through the population and calculates per receptor a gradient from its neighbors' firing rates or first spike latencies. In essence, therefore, with the Gradient Sum method, a single number is arrived at, per sphere, for comparison to that of a second sphere. By comparison in the case of the Euclidean Distance method, one makes receptor to receptor comparisons of population responses elicited by two stimuli. Therefore, the Euclidean Distance method might require the idea of a type of very rapidly decaying "visual store" iconic memory on a per receptor basis. This makes it difficult to see how first spike latencies, in particular, of two indenters would be comparable by a person using this sort of approach. For this reason, only static firing rate was calculated using this method, as opposed to first spike latency,

where the Gradient Sum method's means of creating a single estimate might be more readily comparable between time varying stimuli without the per receptor memory requirement. The Gradient Sum method also more readily affords the use of signal detection theory where the β criterion can be varied to effect larger trial to trial variance. Therefore instead of controlling model variance only by neural noise, which most others have done in the past, we can also model variance due to inconsistent classification.

The study of the population codes used by the brain to discriminate tactile stimuli remains an area of exploration. A number of investigators have sought to align the indentation of the skin's surface with a human psychophysical response. Wheat and Goodwin, for example, extrapolated their single-unit model to a population, whereby factors included receptor density, receptor sensitivity and covariance, and noise [11]. Their simulated population is a regression using a template matching approach, from which an estimate of indenter curvature was attained. In some ways, this approach is similar to the Gradient Sum approach, in that a prediction with some probability is arrived at per indenter for comparison to that of the standard. However, we calculate a per receptor gradient whereas Goodwin and Wheat match a regressed receptor prediction to a recorded firing rate for a known stimulus position on the skin surface. Related is the use of regression models tied to the geometric features of a particular indenter, in contrast to the physics-based model described herein, which was built with a finite element model to enable the predictions of novel stimuli. For example, the single-unit models were fitted to bar and gap stimuli and then used in a population to predict spherical stimuli. The single-unit models also afford an evaluation of population response under dynamic or static firing rate or first spike latency. Another difference is that herein is used a signal detection theory approach that involves the employment of different β criterion values, as noted in the paragraph above, in addition to more standard means to judge discrimination if the distance of the comparison indenter from the standard is half that between the means of these distributions.

In another distinct effort to model population encoding, Guclu and Bolanowski created simulated populations with dependent measures both quantitative (e.g., number of active fibers, summated firing rate, average firing rate) and qualitative (i.e., visual comparisons in plots) to investigate the population response given changes to innervation geometry and receptor density [33]. They then introduced the idea of a "higher order neuron" to make semi-global perceptual judgments based on the firing properties of afferents covering a small area.

4.2 Metrics of Single-Unit Coding

Linked to the means of generating a population response, our model affords the consideration of a variety of single-unit coding metrics. We considered the firing rate in the static hold phase of the indentation, the firing rate in the dynamic ramp, and as well first spike latency. Similarly, given just the timing of first spikes, work by Johansson, et al. have considered the recruitment order of a population of afferents to predict the direction and orientation of indentation, with an empirical model [9].

Among the three measures, our finding was that the firing rate in the static hold was the best predictor, observed in Figure 7 for both the Gradient Sum and Euclidean Distance methods,

because its prediction was robust to the 0.2 mm lateral shift and fit the psychophysical data most closely across the set of indenters. The other measures were reasonable predictors, though there was some discrepancy between predictions given the 0.2 mm small shift. This might not be expected of a robust metric. Because the measures of first spike latency and dynamic firing rate do monotonically increase, however, it could be that such measures give initial rough estimations to be refined later with information obtained in the static hold.

4.3 Accounting for Other Sources of Information

Other significant sources of information may improve the model's psychophysical prediction. In particular, the model herein does not account for input given 1) other afferent types (e.g., rapidly adapting afferents, which though not as spatially acute as SAIs still prominently contribute to form processing and are present at higher densities), 2) near simultaneous use of multiple coding strategies (as suggested via "what" [first spike latency] and "how much" [static and/or dynamic firing rate] information to fit behavioral timescales [9]), and 3) afferent populations located near the nail (SAI afferents along the outline of the nail may resolve the direction of indentation and curvature of the indenter [13]). Concerning the latter, a preliminary analysis in Figure 9 yields high stress concentrations near the nail, indicating that SAIs near the nail may indeed inform a psychophysical prediction, though this was not rigorously attempted here. Further efforts might include these additional sources of information. We note that the ability to examine these types of questions, such as using only those afferents near the edge of the nail, is a benefit of using a multi-level, physics-based modeling approach.

4.4 Model Limitations

While cylinder, bar and sphere indenters were used at different stages of model validation, and tied to existing biological data, work yet remains to differentiate stimuli other than spheres at the psychophysical level. This is planned future work. Also, the models replicate characteristics of the SAI afferent, including more vigorous response during stimulus movement than hold and during greater magnitudes of probe indentation. Its irregular interspike intervals [34] were not a focus as their replication would not greatly impact the population metrics.

Acknowledgment

The work was supported by grants from the Defense Advanced Research Projects Agency (DARPA Grant Number HR0011-08-1-0072) and the National Institutes of Health (NINDS R01NS073119). The content is solely the responsibility of the authors and does not necessarily represent the official views of DARPA or the NIH.

Biographies

Gregory J. Gerling (S’03–M’05) received his Ph.D. degree from the Department of Mechanical and Industrial Engineering at the University of Iowa, Iowa City. He is an Associate Professor in Department of Systems and Information Engineering at the University of Virginia. His research interests include haptics, human factors, computational neuroscience, biomechanics, and human–computer interaction.

Isabelle I. Rivest received her B.S. and M.S. degrees from the Departments of Computer Science, and Systems and Information Engineering, respectively, at the University of Virginia. She is currently at Johns Hopkins Applied Physics Lab in Laurel, MD.

Daine R. Lesniak (S’06) received his B.S. degree in Software Engineering from the University of Wisconsin Platteville and his M.S. and Ph.D. degrees in Systems and Information Engineering from the University of Virginia. He is currently working at Johns Hopkins Applied Physics Lab in Laurel, MD. His interests include computational neuroscience and modeling and simulation.

Jacob R. Scanlon earned his B.S. degrees in Systems and Information Engineering and Mechanical Engineering at the University of Virginia. He is currently pursuing an M.S. degree, after working as an operations research analyst at Booz Allen Hamilton.

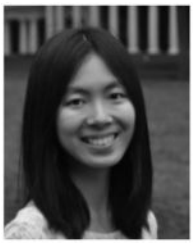

Lingtian Wan received her B.S. degree in Electrical Engineering at the University of Virginia. She is currently pursuing an M.S. degree in Systems and Information Engineering. Her interests include computational neuroscience, bioelectricity and music.

References

[1]. Johnson KO. Neural coding. Neuron. Jun; 2000 26(3):563–566. [PubMed: 10896153]

[2]. Phillips JR, Johnson KO. Tactile spatial resolution. II. neural representation of bars, edges, and gratings in monkey primary afferents. Journal of Neurophysiology. 1981; 46(6):1192–1203. [PubMed: 6275041]

[3]. Gescheider, G. Psychophysics: the fundamentals. 3rd. L. Erlbaum Associates; Mahwah N.J.: 1997.

[4]. Phillips JR, Johnson KO. Tactile spatial resolution. III. A continuum mechanics model of skin predicting mechanoreceptor responses to bars, edges, and gratings. J. Neurophysiol. 1981; 46(6): 1204–25. [PubMed: 7320743]

[5]. Sripati AP, Bensmaia SJ, Johnson KO. A continuum mechanical model of mechanoreceptive afferent responses to indented spatial patterns. J. Neurophysiol. Jun; 2006 95(6):3852–3864. [PubMed: 16481453]

[6]. Dandekar K, Raju BI, Srinivasan MA. 3-D finite-element models of human and monkey fingertips to investigate the mechanics of tactile sense. J. Biomech. Eng.-Trans. ASME. Oct; 2003 125(5): 682–691.

[7]. Freeman AW, Johnson KO. Cutaneous mechanoreceptors in macaque monkey - temporal discharge patterns evoked by vibration, and a receptor model. Journal of Physiology-London. 1982; 323:21–41.

[8]. Bensmaia SJ, Leung YY, Hsiao SS, Johnson KO. Vibratory adaptation of cutaneous mechanoreceptive afferents. J. Neurophysiol. Nov; 2005 94(5):3023–3036. [PubMed: 16014802]

[9]. Johansson RS, Birznieks I. First spikes in ensembles of human tactile afferents code complex spatial fingertip events. Nature Neuroscience. Feb; 2004 7(2):170–177.

[10]. Johnson KO. Reconstruction of population response to a vibratory stimulus in quickly adapting mechanoreceptive afferent fiber population innervating glabrous skin of the monkey. Journal of Neurophysiology. 1974; 37:48–72. [PubMed: 4204567]

[11]. Wheat H, Goodwin A. Tactile discrimination of edge shape: limits on spatial resolution imposed by parameters of the peripheral neural population. Journal of Neuroscience. 2001; 21:7751–7763. [PubMed: 11567065]

[12]. Jenmalm P, Birznieks I, Goodwin AW, Johansson RS. Influence of object shape on responses of human tactile afferents under conditions characteristic of manipulation. European Journal of Neuroscience. 2003; 18(1):164–176. [PubMed: 12859350]

[13]. Birznieks I, Macefield VG, Westling G, Johansson RS. Slowly Adapting Mechanoreceptors in the Borders of the Human Fingernail Encode Fingertip Forces. The Journal of Neuroscience. 2009; 29(29):9370–9379. [PubMed: 19625527]

[14]. Johnson KO. The roles and functions of cutaneous mechanoreceptors. Curr. Opin. Neurobiol. Aug; 2001 11(4):455–461. [PubMed: 11502392]

[15]. Fruhstorfer H, Abel U, Garthe CD, Knuttel A. Thickness of the stratum corneum of the volar fingertips. Clin. Anat. 2000; 13(6):429–433. [PubMed: 11111894]

[16]. Southwood. The Thickness of the Skin. Plastic and Reconstructive Surgery. 1955; 15:423–429. [PubMed: 14384521]

[17]. Wu JZ, Dong RG, Rakheja S, Schopper AW, Smutz WP. A structural fingertip model for simulating of the biomechanics of tactile sensation. Med. Eng. Phys. Mar; 2004 26(2):165–175. [PubMed: 15036184]

[18]. Maeno T, Kobayashi K, Yamazaki N. Relationship between the structure of human finger tissue and the location of tactile receptors. JSME Inter. J. 1998; 41(1):94–100.

[19]. Wagner, M.; Gerling, GJ.; Scanlon, J. Validation of a 3-D finite element human fingerpad model composed of multiple anatomically correct tissue layers; presented at the IEEE Haptic Interfaces for Virtual Environment and Teleoperator Systems; Reno, N.V.. 2008. p. 101-105.

[20]. Goodwin AW, John KT, Marceglia AH. Tactile Discrimination of Curvature by Humans Using Only Cutaneous Information from the Fingerpads. Experimental Brain Research. 1991; 86(3): 663–672. [PubMed: 1761098]

[21]. Guinard D, Usson Y, Guillermet C, Saxod R. Merkel complexes of human digital skin: Three-dimensional imaging with confocal laser microscopy and double immunofluorescence. J. Comp. Neurol. Aug; 1998 398(1):98–104. [PubMed: 9703029]

[22]. Srinivasan MA, Dandekar K. An investigation of the mechanics of tactile sense using two-dimensional models of the primate fingertip. J. Biomech. Eng.-Trans. ASME. Feb; 1996 118(1): 48–55.

[23]. Gerling GJ, Thomas GW. Fingerprint lines may not directly affect SA-I mechanoreceptor response. Somatosens. Mot. Res. 2008; 25(1):61–76. [PubMed: 18344148]

[24]. Khalsa PS, Hoffman AH, Grigg P. Mechanical states encoded by stretch-sensitive neurons in feline joint capsule. Journal of Neurophysiology. Jul; 1996 76(1):175–187. [PubMed: 8836217]

[25]. Ge WQ, Khalsa PS. Encoding of compressive stress during indentation by slowly adapting type i mechanoreceptors in rat hairy skin. J. Neurophysiol. Apr; 2002 87(4):1686–1693. [PubMed: 11929890]

[26]. Lesniak DR, Gerling GJ. Predicting SA-I mechanoreceptor spike times with a skin-neuron model. Math. Biosci. Jul; 2009 220(1):15–23. [PubMed: 19362097]

[27]. Nicholls, JG.; Martin, AR.; Wallace, BG.; Fuchs. From Neuron to Brain: A Cellular and Molecular Approach to the Function of the Nervous System. 4th. Sinauer Associates; Sunderland Mass.: 2001.

[28]. Johansson RS, Vallbo AB. Tactile Sensibility in the Human Hand - Relative and Absolute Densities of 4 Types of Mechanoreceptive Units in Glabrous Skin. Journal of Physiology-London. 1979; 286(JAN):283–300.

[29]. Rivest, I. Validating a model of tactile mechanotransduction to evaluate sparse populations of SAI receptors for activities of daily living. The University of Virginia; 2010.

[30]. Srinivasan MA. Surface deflection of primate fingertip under line load. Journal of Biomechanics. 1989; 22(4):343–9. [PubMed: 2745468]

[31]. Dandekar, K. Role of mechanics in tactile sensing of shape. MIT; Cambridge, MA, USA: 1995.

[32]. Myers, R.; Montgomery, DC. Response surface methodology?: process and product optimization using designed experiments. Wiley; New York: 1995.

[33]. Guclu B, Bolanowski SJ. Modeling population responses of rapidly-adapting mechanoreceptive fibers. Journal of Computational Neuroscience. Apr.2002 12:201–218. [PubMed: 12142551]

[34]. Wellnitz SA, Lesniak DR, Gerling GJ, Lumpkin EA. The regularity of sustained firing reveals two populations of slowly adapting touch receptors in mouse hairy skin. J. Neurophysiol. Apr; 2010 103(6):3378–3388. [PubMed: 20393068]

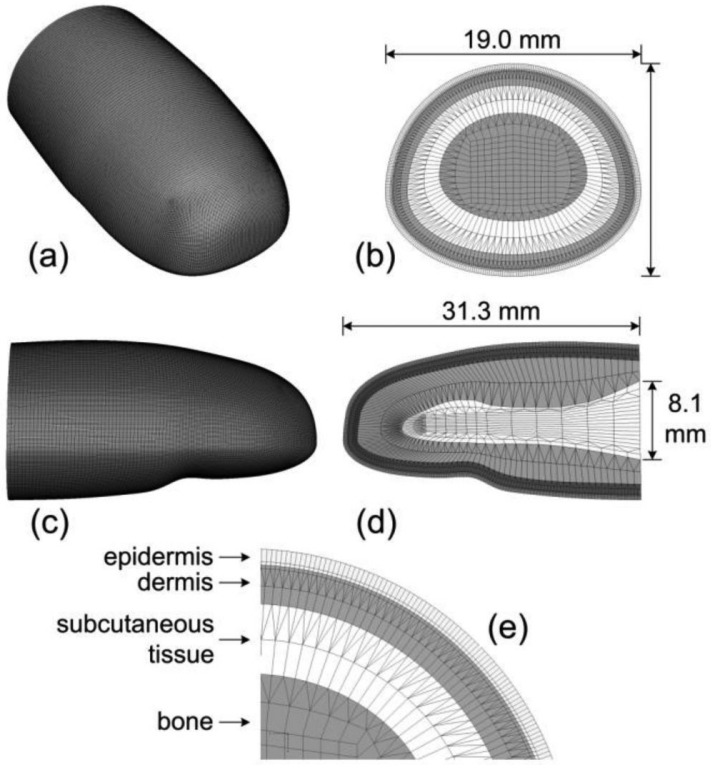

Figure 1.

3D FE mesh of human distal phalange. Shown are the (a) overall mesh, (b) cross section of the mesh near the interconnect with the middle phalange, (c – d) longitudinal section for both the outer surface and inner mesh, and (e) four layers of microstructures. In (e) the epidermis is 0.471 mm thick (0.371 mm stratum corneum and 0.1 mm living epidermis) and the dermis is 1.153 mm thick.

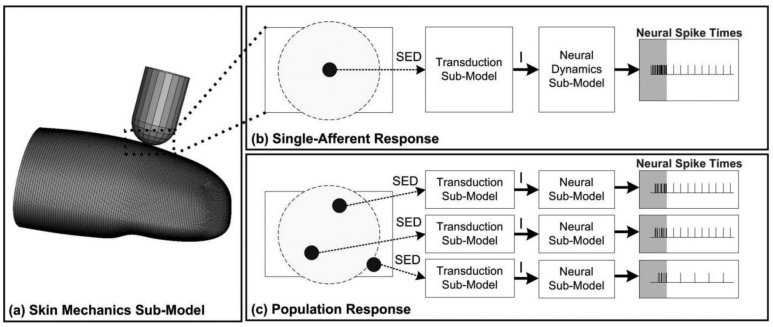

Figure 2.

The model was validated at each of three points; the skin mechanics sub-model, single SAI electrophysiological response, and population response. (a) shows the indentation of a spherical stimulus into the skin mechanics model, (b) denotes the response in neural spike times for a single afferent directly underneath the sphere, and (c) shows the response from a population of 3 afferents. The shaded region under “Neural Spike Times” signifies the 50 ms timeframe in which the indenter was moving into the skin.

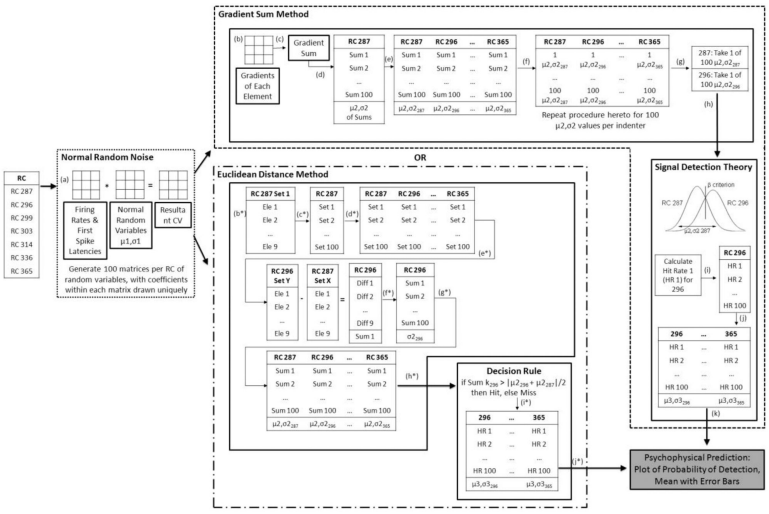

Figure 3.

Steps in probabilistic discrimination of 7 indenters (RC = radius of curvature) at the simulated psychophysical level. Model inputs are firing rate and first spike latency predictions from 18 receptors in a 100 receptor/cm^2 density (though only 9 elements are shown here in (b*) and (e*) due to symmetry). First, noise is applied, then either the Gradient Sum or Euclidean Distance approach, before com-paring the predictions with either Signal Detection Theory or a Decision Rule. Additional details in 2.2.3 Population validation at psychophysical level.

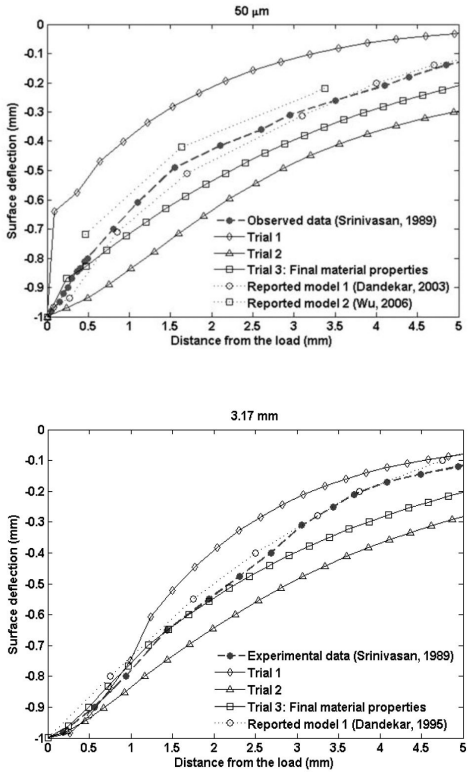

Figure 4.

Skin surface deflection of the FEM in response to a 50 μm line load (upper) and a 3.17 mm diameter cylinder (lower) indented to a depth of 1.0 mm.

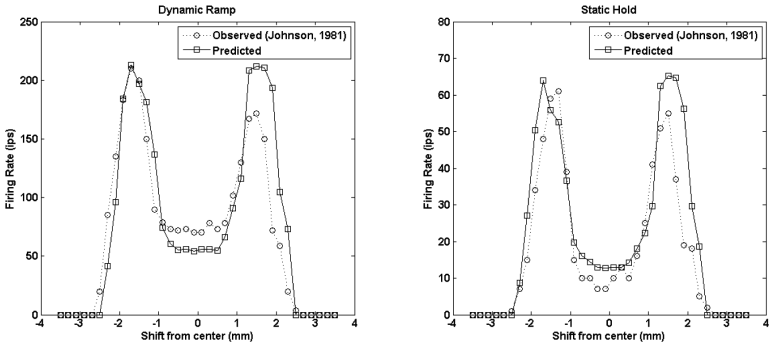

Figure 5.

Plot of predicted and observed firing rates in dynamic ramp (left) and static hold (right) phases for a 3.0 mm bar indented at various lateral shift locations relative to the SAI receptive field center. Observed firing rates recorded by Phillips and Johnson, 1981.

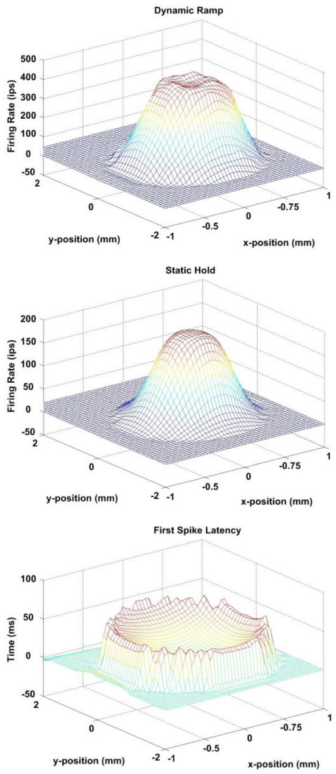

Figure 6.

3D plots of predicted firing rates in the dynamic phase (upper) and in the static hold (middle) phase for a population of receptors when indented with a spherical stimulus of curvature 287 m^{-1}. Also shown is first spike latency (lower).

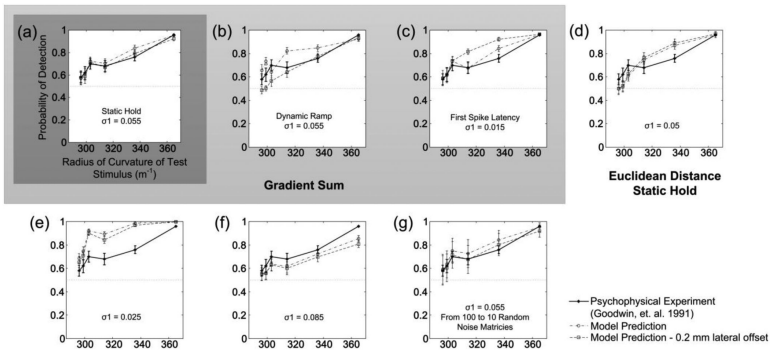

Figure 7.

Psychophysical predictions of firing rate during the (a) static hold phase (b) dynamic ramp phase of the indentation, and using (c) first spike latency. Plot (d) shows the prediction using the Euclidean Distance method. In plots (e) and (f) the Gradient Sum method was used to calculate static firing rate where noise level was varied at 0.025 and 0.085, on either side of the 0.055 in (a). The best fit of the mean psychophysical data from Goodwin, 1991 was found in (a) at a noise level of 0.055. In plot (g), only 10 random noise matrices were used instead of the 100 as in all other simulations. Note that the standard indenter was 287 m^{-1}.

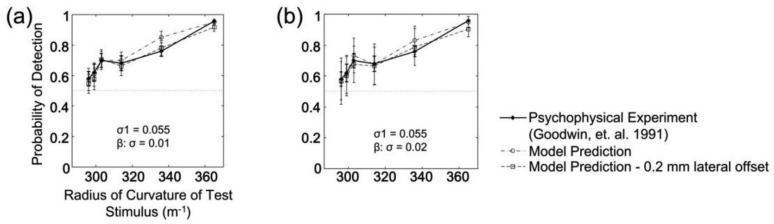

Figure 8.

Psychophysical predictions using the Gradient Sum method to control the estimation of the error bars by changing the β criterion a small amount from trial to trial using signal detection theory. The standard deviation of the distribution from which β was drawn increased from 0.01 in plot (a) to 0.02 in plot (b) which increased the error bars but left the means unchanged.

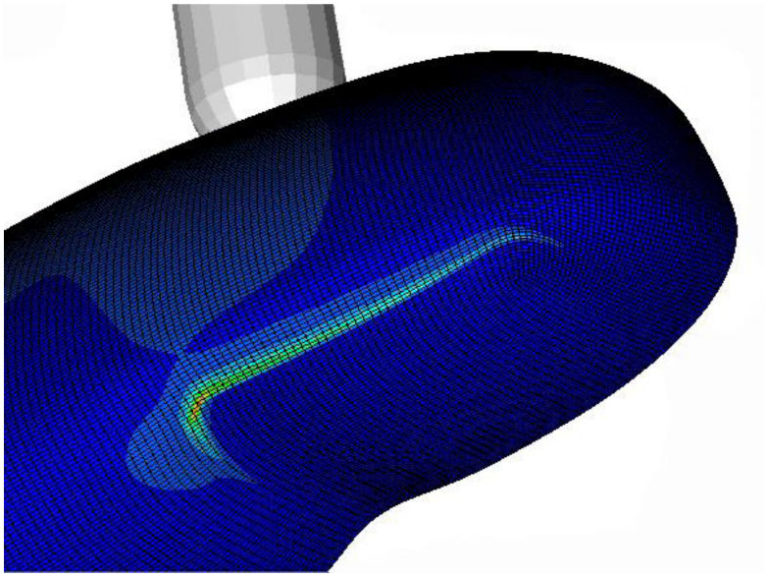

Figure 9.
Finite element model deformed by a sphere stimulus, whereby high stresses are indicated at the border of the nail.

Table 1

FEM material properties from Maeno, et.al. [18].

Skin Layer	E (Pa)	v
Epidermis, Trial 1	1.36×10^5	0.48
Dermis, Trial 1	8.00×10^4	0.48
Subcutaneous tissue, Trial 1	3.40×10^4	0.48
Bone, Trial 1	1.70×10^7	0.48

Table 2

Parameters for the material properties in Trial 2, from Wu, et al. [17].

Skin Layer	E (Pa)	*v*	C10 (Pa)	C01 (Pa)	C20 (Pa)	C11 (Pa)	C02 (Pa)	D1 (Pa^{-1})	Temp (°C)
Epidermis, Trial 2	2.00×10^6	0.30	-	-	-	-	-	-	-
Dermis, Trial 2	-	-	2430	5420	239000	−262000	74700	13.3	25
Subcutaneous tissue, Trial 2	-	-	300	671	29800	−32700	9330	106.5	25
Bone, Trial 1	1.70×10^7	0.30	-	-	-	-	-	-	-

Table 3

Testing and training sets for cross validation. Data points represent the lateral shifts of the indenter from the center directly above the indenter being location 0.0. Values are in units mm.

Fold 1

Testing	Training	Training	Training	Training	Training
−3.3, -1.3, −0.3 0.9, 1.5, 2.3	−2.5, −1.9, −0.9, 0.5, 2.5, 3.5	−3.1, −1.5, −0.7, −0.1, 1.1, 2.1	−2.9, −2.3, −1.1, 0.1, 1.7, 2.7	−3.5, −2.1, −0.5, 1.3, 2.9, 3.3	−2.7, −1.7, 0.3, 0.7, 1.9, 3.1

Fold 6

Training	Training	Training	Training	Training	Testing
−3.3, −1.3, −0.3 0.9, 1.5, 2.3	−2.5, −1.9, −0.9, 0.5, 2.5, 3.5	−3.1, −1.5, −0.7, −0.1, 1.1, 2.1	−2.9, −2.3, −1.1, 0.1, 1.7, 2.7	−3.5, −2.1, −0.5, 1.3, 2.9, 3.3	−2.7, −1.7, 0.3, 0.7, 1.9, 3.1

Table 4

Model parameters and corresponding FSS obtained at each step of the RSM model fitting for the fold 3, start point 2. At the final iteration, the out-of-sample FSS was 0.837.

Iteration	Model Parameters						in-sample FSS
	β (mA)	k_d (mA · Pa/ms)	k_s (mA/Pa)	τ (ms)	C (mF)	$\bar{v}$ (mV)	
0 (Start)	0	3.00E-07	8.20E-09	68.00	1.00E-06	50.00	0.7748
1	−8.13E-09	3.07E-07	7.88E-09	67.49	1.01E-06	50.04	0.8160
2	−8.77E-09	3.08E-07	7.87E-09	67.32	1.01E-06	50.06	0.8175
3	−1.05E-08	3.16E-07	7.85E-09	66.84	1.01E-06	50.10	0.8226
4	−1.06E-08	3.16E-07	7.84E-09	66.80	1.01E-06	50.10	0.8233
5	−1.07E-08	3.16E-07	7.84E-09	66.77	1.01E-06	50.10	0.8234
6 (Final)	**−1.07E-08**	**3.16E-07**	**7.84E-09**	**66.77**	**1.01E-06**	**50.10**	**0.8234**

Table 5

Predicted modulation indices, compared to those recorded *in vivo* for Phillips and Johnson, 1981 [4].

	dynamic firing rate (spikes/sec)			static firing rate (spikes/sec)		
	min	**max**	**m**	**min**	**max**	**m**
Predicted	54	212	0.59	13	65	0.67
Johnson, 1981	70	210	0.50	7	61	0.79